Nuclear Hyperfine Interaction in ^{141}Pr†

M. F. Bent, D. D. Cook, and B. I. Persson
California Institute of Technology, Pasadena, California 91109
(Received 19 October 1970)

Nuclear hyperfine interactions in the 145-keV state of ^{141}Pr have been investigated by measurements on Mössbauer-scattered γ rays. The magnetic moment of this level was determined to be $2.78^{+0.12}_{-0.06}\mu_N$, a value which is considerably larger than that predicted by Kisslinger and Sorensen. Renormalizing g_l in their calculation to account for meson-exchange effects reduces the disagreement significantly. The magnetic field at the site of the Pr nucleus has been investigated for a number of compounds. The values 2.07 ± 0.08 and 0.86 ± 0.06 MOe were obtained for the fields at 4.2°K in PrB_6 and PrO_2, respectively. Although these are only about $\frac{1}{2}$ the values expected for the internal fields in the corresponding free Pr ions, the temperature dependence closely followed a Brillouin function. Line broadening that persisted to temperatures well above the magnetic-ordering temperatures was observed for these compounds indicating the presence of a smaller residual hyperfine interaction. Isomer shifts have been observed for a number of Pr compounds. Based on isomer shifts between ionic trivalent and tetravalent compounds, the difference in the mean square charge radii of the excited and ground states is estimated: $\langle r_e^2\rangle - \langle r_g^2\rangle = (6.3 \pm 2.5) \times 10^{-3}$ fm^2.

INTRODUCTION

Mössbauer scattering techniques have been used to study hyperfine interactions in the 145-keV state ($I^\pi = \frac{7}{2}^+$) and ground state ($I^\pi = \frac{5}{2}^+$) of ^{141}Pr. The transition is nearly pure $M1$ (<0.4% $E2$) and the measured half-life[1] of the excited state ($t_{1/2}$ =1.9 nsec) gives a minimum width (2Γ) of 0.98 mm/sec for the resonance.

Scattering experiments are particularly well suited for this transition. The fraction of γ rays that are scattered resonantly can be much larger than the f factor of the source ($f_s < 0.5\%$ at 4.2°K) which is an upper bound for the effect, i.e., |1 − (counting rate on resonance)/(counting rate off resonance)|, observable in transmission. The maximum effect in scattering is given by $f_s\sigma_M/(f_s\sigma_M + \sigma_R)$ where σ_M and σ_R are the Mössbauer and Rayleigh scattering cross sections. In the present case $f_s\sigma_M$ and σ_R have comparable values for compounds with sufficiently high Debye temperatures ($\theta_D > 175$°K), and observable effects up to 50% may be expected.

Mössbauer scattering in ^{141}Pr was first reported by Debrunner and Frauenfelder.[2] They used CeO_2 and CeF_3 sources and a Pr_6O_{11} scatterer at 16°K. No hyperfine splitting was observed.

Nuclear Zeeman splittings corresponding to calculated values[3] of the internal fields in Pr^{3+} and Pr^{4+} ions are large compared with the natural line width, and well-resolved Mössbauer spectra are expected. Magnetic splitting in tetravalent PrO_2 at 4.2°K has been reported[4] by the authors. The spectra were only partially resolved, however, and the parameters of the hyperfine interaction were determined with poor precision. Since larger splittings are expected for Pr^{3+} ions, a search was made for tightly bound trivalent compounds which are ordered at accessible temperatures. Well-resolved spectra were obtained for PrB_6 and $PrAl_2$ at 4.2°K, and accurate values of the internal field and g-factor ratio were determined from the former data. Bulk-susceptibility measurements[5] indicate magnetic ordering in other trivalent compounds above 4.2°K, but no evidence of magnetic hyperfine interaction was seen in several such compounds.

In compounds in which the exchange coupling between rare-earth ions is strong enough to produce magnetic ordering, the internal fields are usually observed to be close to the free-ion fields. Since the internal fields in antiferromagnetic PrB_6 and PrO_2 and in ferromagnetic $PrAl_2$ were found to be only about $\frac{1}{2}$ the free-ion fields, the temperature dependence of the hyperfine interaction might also be expected to deviate from free-ion behavior. The internal fields in the former two compounds were found, however, to approximately follow Brillouin functions, but the Néel temperature deduced for PrB_6 was considerably larger than the previously reported value.[6]

Isomer shifts are usually small and difficult to interpret for sixth-period elements because most of these elements display only a single valence in ionic compounds. In Pr, however, it was possible to measure isomer shifts in largely ionic tetravalent and trivalent compounds. Since the electronic configurations of these ions differ by only a $4f$ electron, estimates of the difference in electron density at the nucleus were possible, and the rela-

tive isomer shifts were used to evaluate the change in the nuclear-charge radius accompanying the transition.

EXPERIMENT

For the present experiments a vertical transmission spectrometer, which has previously been described,[7] was converted into the scattering spectrometer shown in Fig. 1. A tungsten collimator at the bottom of the tube enclosing the drive system served to support the sources, to collimate the scattered radiation, and to shield the detector from direct radiation. The use of several identical sources evenly spaced around the axis of the collimator largely eliminated any disturbing effects from nonuniformities and small lateral displacements of the scatterer. The scattering material was crushed to a powder and uniformly dispersed in wax, then pressed into a cylindrical aluminum holder $\frac{3}{4}$ in. in diameter and $\frac{3}{8}$ in. deep. The scatterer holder was mounted on the lower end of a rod driven by a constant-acceleration drive.[8] About 0.6 g/cm^2 of Pr was normally used; this produces negligible thickness broadening.

Scatterer temperatures were measured with a small carbon resistor embedded in the scattering material. Temperatures below 4.2°K were obtained by pumping to lower the pressure above the helium bath. A liquid-nitrogen bath was used for the measurements at 77°K. In these cases the scatterer and the source had the same temperature. In other runs the source remained at 4.2°K while the scatterer was heated.

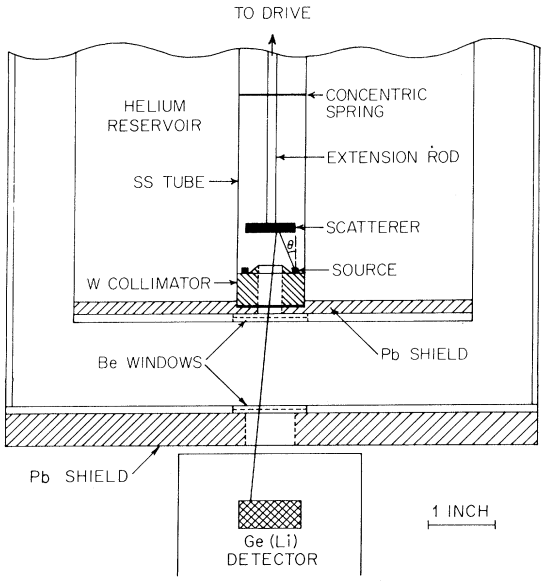

FIG. 1. Scale drawing of the experimental arrangement for the most frequently used source-scatterer distance ($\langle\cos\theta\rangle=0.87$). Twice this distance ($\langle\cos\theta\rangle=0.96$) was used for some measurements to decrease velocity dispersion. The angle between the direction of an emitted γ ray and the velocity of the scatterer is designated by θ.

Most of the nonresonant radiation striking the detector resulted from Compton scattering of 145-keV γ rays by the scatterer. With the back-scattering arrangement used, the Compton peak is degraded in energy by nearly 50 keV and is easily separated from the resonantly scattered γ rays. The source-scatterer distance was chosen to give the largest solid angle possible without undue broadening (<20%) of any component in the spectrum by velocity dispersion (cf. Appendix). The collimator design chosen does not screen off the central portion of the detector and makes efficient use of the comparatively small active area of the Ge(Li) detector (1.5-cm radius×1.1-cm depth). The good resolution (1.7 keV at 145 keV) of this detector allowed a narrow window to be set on the scattered peak, thereby excluding most of the Compton-scattered contaminant radiation. The large resonant effect observable with a Ge(Li) detector more than compensates for the small product solid angle (0.025%) obtained.

With the present geometry, velocity dispersion results in a more complicated functional form for the components of the Mössbauer spectrum than is observed with geometries, such as that used in Ref. 2, which have axial symmetry about a point source. In addition to the primary data, velocity spectra were measured with a ^{57}Co source and a scatterer of enriched Fe_2O_3 using the scattering geometry shown in Fig. 1. The Fe_2O_3 spectrum is more sensitive to velocity dispersion effects than the Pr spectra are and was used to check the velocity calibration and the line shape used in fitting the data. Several praseodymium spectra were obtained with less velocity dispersion by increasing the source-scatterer distance or by decreasing the diameter of the scatterer, but with a sacrifice in the counting rate.

Sources used in the experiments were obtained by neutron irradiation of 20-mg quantities of CeO_2, enriched to 99.7% ^{140}Ce, sealed in small aluminum cans. 1-month irradiations with a neutron flux of 4×10^{14} cm^2 sec^{-1} produced about 50 mCi of ^{141}Ce ($t_{1/2}=33$ days) per can. Up to eight cans were used at one time. The decay of ^{141}Ce populates only the 145-keV state of ^{141}Pr, and the direct energy spectrum of the sources showed the total intensity of high-energy contaminants to be less than 0.3%. The scattered peak (Mössbauer plus Rayleigh) was about nine times more intense than the Compton background from high-energy contaminants. The large effects observed (up to 20%) in

peaks having a width $\sim 2 \times 2\Gamma$ are accounted for quite well in terms of the expected ratio of Mössbauer to Rayleigh scattering; the Compton background included did not attenuate the effect by more than 10%.

Compounds giving both magnetically split and single-line spectra were used as scatterers, praseodymium dioxide and hexaboride being the most thoroughly studied magnetic materials. Samples of PrO_2 were prepared from lower oxides by valence disproportionation and by high-pressure oxidation. In the first procedure Pr_6O_{11} was repeatedly leached in boiling water and acetic acid for two days. The final product is not pure PrO_2, but probably $PrO_{1.95}$.[9] Purer PrO_2 was prepared[10] by heating Pr_6O_{11} to 400°C in oxygen at 185 atm. The composition of the material was found to be $PrO_{2.002(5)}$. X-ray analysis indicated a CaF_2 structure with a lattice constant $a_0 = 5.393(2)$ Å.

Samples of PrB_6 were prepared from pressed pellets containing stoichiometric amounts of 99.9% pure amorphous boron powder and 99.8% pure Pr metal filings. The pellets (~5 g) were first partially reacted by induction heating under an inert atmosphere to avoid loss of material, then repeatedly arc-melted to give homogeneous compact samples which were subsequently crushed. X-ray analysis of the material used indicated a majority phase (>97%) having a cubic CaB_6 structure [$a_0 = 4.133(5)$ Å] and a single minority phase, probably PrB_4, having the tetragonal TbB_4 structure with $a_0 = 7.20(2)$ Å. No oxide phase was detected.

Several other compounds which were expected to show magnetic ordering at 4.2°K were also investigated. The Laves phase compounds $PrAl_2$, $PrRu_2$, and $PrIr_2$, prepared by levitational melting, were used but the observed effects were very small. The monochalcogenides PrN, PrS, and $Pr_xLn_{1-x}S$ (Ln = another lanthanide) with the cubic NaCl structure were also studied. The sulfides were made by gradually heating stoichiometric amounts of the elements to about 400°C in sealed quartz ampoules, pressing the resulting powders into pellets, and finally arc-melting the pellets. PrN samples were prepared by heating Pr metal in purified N_2 and NH_3 gases and by thermal decomposition of $Pr(CN)_3$ and $Pr_2(NCN)_3$. Only those monochalcogenide compounds containing magnetic rare earths (Gd or Dy) showed hyperfine splitting. The additional Rayleigh scattering from these nuclei, when included in sufficient concentrations to give large splittings, decreased the observed effect so that useful spectra were not obtained. Similar behavior was observed in $PrPO_4$ and $Pr_xLn_{1-x}PO_4$. These anhydrous phosphates were prepared by dessicating the precipitated hydrated salts. Magnetic splitting was observed in PrC_2, but this compound is so reactive that contamination and deterioration of the samples occurred.

The spectra of several materials which give single lines at 4.2°K were also measured to set an upper limit for the line width of the source and to investigate isomer shifts. Pr_2O_3 was prepared by heating Pr_6O_{11} in vacuum at 1000°C for 12 h. Commercially obtained Pr_2S_3, PrF_3, and $PrFeO_3$ were also studied.

RESULTS AND ANALYSIS

The width and area of the scattered peak observed in the velocity spectra of a number of compounds at 4.2°K are given in Table I. Isomer shifts relative to a CeO_2 source and hyperfine magnetic fields in these materials are also summarized. Some materials not listed in this table (e.g., $PrFe_2$, $PrIr_2$, $PrRu_2$, Pr metal) were also investigated but the small effects (<1%) prevented accumulation of useful data. The smallest line width (2.0 ± 0.1 mm/sec) was observed for the nonmagnetic Pr_2O_3, whereas the natural line width (2Γ) is 0.98 mm/sec.

Hyperfine Interactions at 4.2 and 2.0°K

Although evidence of a magnetic hyperfine interaction at 4.2°K was observed for a number of compounds, only in the case of PrB_6, PrO_2, and $PrAl_2$ were the spectra reasonably well resolved. For $PrAl_2$ the observed effect was only about a $\frac{1}{10}$ of that for the other materials, rendering this data useless for determining the g-factor ratio.

The four PrB_6 spectra shown in Fig. 2 and four PrO_2 spectra obtained under similar conditions (F and G in Fig. 3 are representative) were analyzed to determine this quantity. The same scatterer was used in the four measurements for each compound, but the scattering geometry, velocity range, or scatterer temperatures differed as indicated in the figures.

Theoretical curves were fitted to the velocity spectra of each material in a combined least-squares procedure.[11] A functional form which accounts for the effects of velocity dispersion [cf. Appendix, Eq. (3)] was used. In the following discussion, this compensation for geometric distortion is implicit, and the parameters used are those that would be employed in fitting thin-absorber transmission spectra. The hyperfine components are assumed to be Lorentzian with relative intensities given by the theoretical transition probabilities. Allowance was made for the difference in Boltzmann population of the ground-state Zeeman levels (amounting to as much as 30% in PrB_6 at 2°K). The area effect, isomer shift, g-factor ratio (g_e/g_g), and width of corresponding components were assumed to have the same value

for each material. The solid curves for spectra A–D, F and G correspond to the best fits obtained with these assumptions. The solid curves in the upper part of Fig. 4 show the normalized χ^2 obtained in fits in which the g-factor ratio was fixed to various values while the other parameters were allowed to vary subject to the above constraints.

Very poor fits ($\chi^2 > 5$) result if all the hyperfine components are assumed to have the natural line width. For both materials, better fits ($\chi^2_{PrB_6} \approx 2.5$ and $\chi^2_{PrO_2} \approx 3.0$) are obtained when the width of the components is allowed to increase to about 4 mm/sec. However, the best fits ($\chi^2_{PrB_6} \approx 1.4$ and $\chi^2_{PrO_2} \approx 1.2$) require that the width of the outer lines in the spectra be greater than the width of the inner lines. In the fits described above, the component line width was assumed to have the form $W = W_0 + \alpha \Delta E_{mag}$, where W_0 is the width of a fictitious line at zero velocity, α is an adjustable constant, and ΔE_{mag} is the absolute value of the observed displacement due to the magnetic interaction. For PrB_6 the best fit, giving $g_e/g_g = 0.48$, is obtained with $W_0 = 3.25$ mm/sec and $\alpha = 0.06$. Since this broadening could not be explained with certainty, the PrB_6 spectra were fitted using theoretical functions which spanned the range of plausible forms of the broadening. A wide variety of component line shapes both symmetric and asymmetric (cf. Appendix) as well as functional forms corresponding to various numbers of magnetically inequivalent lattice sites were tried. The value of χ^2 is not improved for any value of g_e/g_g by the introduction of parameters which produce symmetric broadening of the lines. Parameters giving asymmetric lines or site populations can slightly improve the fits for some values of g_e/g_g. In no case, however, is the value of g_e/g_g which best fits the data changed by more than a fraction of a standard deviation nor is the fit at this point improved.

In Fig. 5 the effects of including quadrupole interactions [electric field gradient (EFG) collinear with H_{int}] in the analysis are shown. The dashed curves show the variation in χ^2 and g_e/g_g when the PrB_6 data was fitted assuming various values for the excited-state quadrupole splitting ($Q_e V_{zz}$). The effect on the value of g_e/g_g is negligible and an upper limit $Q_e V_{zz} \lesssim 0.8$ mm/sec is indicated. The components of the magnetically split spectra do not have the natural width; therefore, the determined g-factor ratio may depend on the widths assumed for the components. The solid curves in Fig. 5 show the value of the g-factor ratio which best fits the PrB_6 data and the χ^2 obtained when various fixed component widths are used. The χ^2 curves plotted in Figs. 4 and 5 represent the intersection of a multidimensional χ^2 surface with planes parallel to various coordinate axes and were used to establish confidence limits for the various parameters. The number of degrees of freedom in the fits was ~300. An increase in χ^2 by 0.08 then corresponds to 1 standard deviation

TABLE I. Properties of some praseodymium compounds at 4.2°K.

Compounds	Isomer shift [a] (mm/sec)	Area effect [b] (%×mm/sec)	H_{int} (MOe)	Width (mm/sec)	Magnetic-ordering temp.[c] (°K)
PrB_6	−0.31 ± 0.03	170	2.07 ± 0.08	2.2 ± 0.3 [d]	7.5
$PrAl_2$	−0.31 ± 0.15	12	1.7 ± 0.4	5 ± 2	34
PrO_2	+0.62 ± 0.05	220	0.85 ± 0.04	2.8 ± 0.6 [d]	14
Pr_6O_{11}	+0.61 ± 0.07	90		3.6 ± 0.1	
Pr_2O_3	−0.14 ± 0.03	40		2.0 ± 0.1	
PrF_3	−0.36 ± 0.06	60		3.2 ± 0.2	<4.2
$PrPO_4$	−0.10 ± 0.07	100		2.9 ± 0.2	
PrC_2	−0.4 ± 0.4	30	e	8.8 ± 1.5	15
$PrFeO_3$	+0.30 ± 0.05	90		4.1 ± 0.1	
PrS	−0.08 ± 0.07	70		3.6 ± 0.6	16
Pr_2S_3	−0.11 ± 0.05	70		3.1 ± 0.5	
$Pr_{0.5}Gd_{0.5}S$	−0.12 ± 0.09	20	e	5.2 ± 0.7	
PrN	−0.10 ± 0.08	50		3.3 ± 0.2	
$Pr_{0.5}Dy_{0.5}PO_4$	−0.19 ± 0.11	30	e	5.9 ± 0.9	

[a] Relative to CeO_2 source.

[b] The numbers listed are the ratios (expressed in percent) of resonantly scattered events in the whole spectrum divided by the number of nonresonant background events in a velocity interval of 1 mm/sec. In all cases the scatterer thickness was about 600 mg/cm^2 of ^{141}Pr.

[c] Temperatures below which the material is reported to show bulk magnetization. These are not results of the present experiments. Individual references are given in Ref. 5.

[d] At 77°K.

[e] The considerably broadened line indicates the presence of a magnetic hyperfine interaction.

in a parameter (cf. the horizontal lines in Figs. 4 and 5). Since errors from other sources than those discussed are much smaller, we obtain

$$g_e/g_g = +0.48^{+0.02}_{-0.01},$$

where the errors correspond to two standard deviations. The PrO_2 spectrum gives the consistent but less accurate value 0.50 ± 0.05. Using the value $\mu(\frac{5}{2}) = +4.136(4)\mu_N$ for the ground-state moment,[12] one obtains for the excited-state moment

$$\mu(\tfrac{7}{2}) = 2.78^{+0.12}_{-0.06}\,\mu_N$$

and the values of the internal magnetic fields listed in Table I. In addition to statistical errors, the errors quoted include the effects of uncertainties in geometry and errors in the drive motion, but the main contribution is due to uncertainties in the origin of the unresolved hyperfine interaction which broadens the lines.

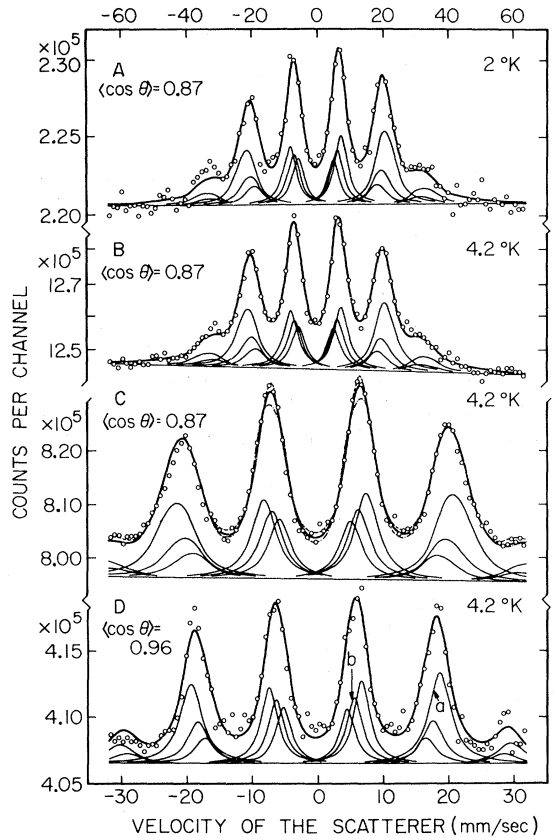

FIG. 2. The velocity spectra of PrB_6 which were used for the determination of g_e/g_g, the ratio of the g factors of the excited and ground states. These spectra have been obtained for the two velocity ranges shown and for different geometries as indicated by $\langle\cos\theta\rangle$. The solid curves represent the best combined fit to the data and the corresponding Zeeman components are shown. The dashed and dot-dash curves shown for spectrum C correspond to the best combined fit obtained with the g-factor ratio fixed to 0.50 and 0.465, respectively.

Temperature Dependence of the Internal Fields

Representative velocity spectra of PrB_6 and PrO_2 in the temperature range 2–77°K are shown in Figs. 3 and 6. The values obtained for the internal fields at the Pr nuclei in the two materials as a function of temperature are shown in Fig. 7. At 77°K the widths of the peaks are similar to those observed for nonmagnetic compounds at 4.2°K (cf. Table I). Just above the ordering temperature, where the main part of the hyperfine interaction vanishes, the widths of the spectra are considerably greater (~4.5 mm/sec) than at 77°K and are closer to the average width of the components in the resolved spectra below the ordering temperatures. Near the ordering temperatures the spectra are too poorly resolved to obtain both the magnetic splitting and the width of the components by fitting the data. To obtain values for the internal fields in this region the average widths of the com-

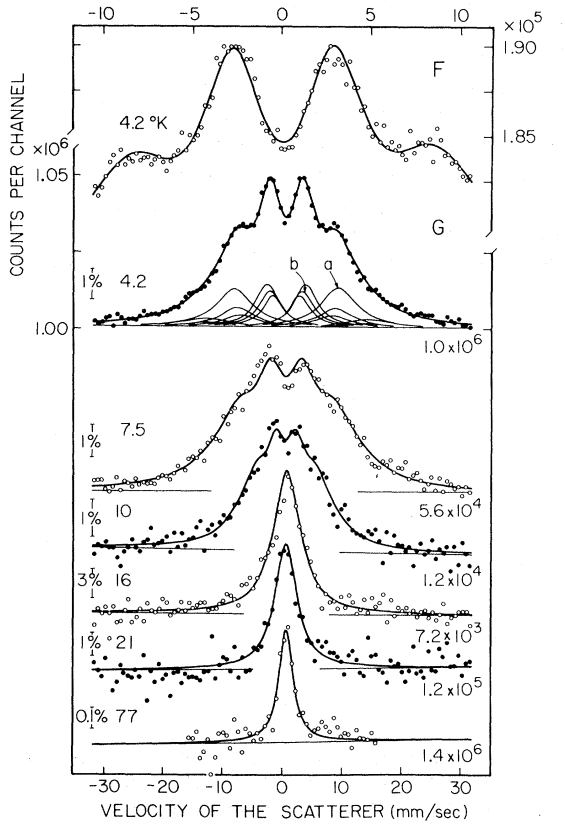

FIG. 3. Velocity spectra for PrO_2. Spectra F and G were used in determining the g-factor ratio g_e/g_g. The spectrum F was obtained with the velocity range reduced to $\frac{1}{3}$ of that for the other spectra. The lower part of the diagram shows the temperature dependence of the hyperfine spectrum (labeled as in Fig. 6. same fashion as Fig. 6.

ponents were fixed to interpolated values. The curves shown in the figure are Brillouin functions fitted to the data. Ordering temperatures of 19.8 ± 0.9°K for PrB_6 and 12.4 ± 1.1°K for PrO_2 are then obtained.

DISCUSSION

Nuclear Moments

Arima and Horie[13] were the first to point out that the magnetic and quadrupole moments of the ^{141}Pr ground state could be accounted for on the basis of configuration mixing of single-particle states and that the proton configuration was more likely $(1g_{7/2})^6(2d_{5/2})^3$ than $(1g_{7/2})^8(2d_{5/2})^1$. According to Kisslinger and Sorensen[14] the collective contribution to the ground- and excited-state magnetic moments of ^{141}Pr is negligible and calculations involving only configuration mixing should be sufficient. They predicted $4.02\mu_N$ for the magnetic moment of the ground state, in good agreement with the experimental value of $4.14\mu_N$. However, their prediction of $2.00\mu_N$ for the magnetic moment of the excited state is considerably smaller than the measured value $2.78\mu_N$.

The situation closely resembles that of ^{139}La. The ground-state spin of ^{139}La is $\frac{7}{2}$ and its proton and neutron configurations are those of ^{141}Pr with a pair of protons removed. Collective contributions in ^{139}La, as in ^{141}Pr, are believed to be negligible, and the magnetic moment of the ground state of ^{139}La is predicted[14] to be $2.25\mu_N$ in disagreement with the experimental value[12] of $2.78\mu_N$.

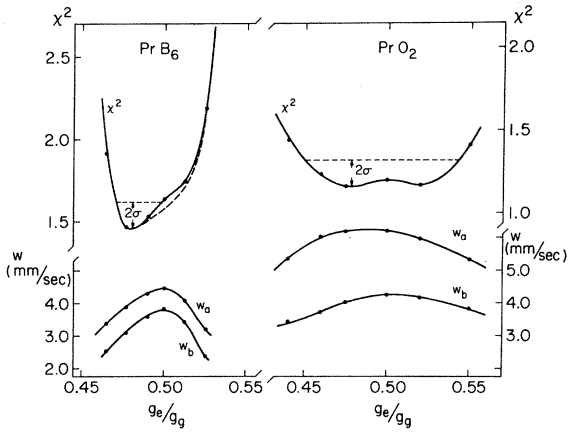

FIG. 4. Dependence upon the g-factor ratio of χ^2 and the widths of representative Zeeman components for PrB_6 and PrO_2. The widths of the components labeled a and b in spectra D and G are designated by w_a and w_b. The dashed lines indicate the two standard deviation confidence limit for the g-factor ratio. The solid curves were obtained assuming a symmetric distribution of internal magnetic fields. The dashed curve for PrB_6 was obtained for the asymmetric distribution of the fields that gave the smallest χ^2 (cf. text).

To account for the magnetic moment of the ground state of ^{141}Pr on the basis of the extreme single-particle model, assuming $g_l = 1.0$, requires an effective proton g factor g_s of $0.75g_{\text{free}}$. The experimental value 0.48 for g_e/g_g implies that the effective proton g factor in the excited state should be $0.52g_{\text{free}}$. If one instead determines the values of g_l and g_s which would give the experimental values of the two magnetic moments, one finds $g_s = 0.69g_{\text{free}}$ and $g_l = 1.1$. This value for g_l is reasonable on the basis of meson exchange.[15]

The magnetic-moment calculation of Kisslinger and Sorensen with this renormalization of g_l gives $\mu(\frac{7}{2}) = 2.4\mu_N$ and $\mu(\frac{5}{2}) = 4.2\mu_N$, in better agreement with the experiment. In addition, the magnetic-moment operator should include a term of the form $K(\sigma Y_2)$, due to meson exchange,[15] where $K \approx -1$. Including it changes the above values for $\mu(\frac{7}{2})$ and $\mu(\frac{5}{2})$ to $2.46\mu_N$ and $4.15\mu_N$, respectively, which further improves the agreement with experimental values.

The quadrupole moment of the ground state[12] is so small [0.0589 (5) b] that quadrupole splittings observable in Mössbauer spectra must occur mainly in the excited state. On the basis of the quadrupole splittings observed in isostructural rare-earth compounds, lower limits of 2×10^{18} V/cm² and $(2.5-3.5)\times10^{18}$ V/cm² are expected for the EFG at the nucleus in cubic PrB_6 and in noncubic Pr_2O_3 and PrF_3, respectively. The upper limit of 0.8 mm/sec for the quadrupole splitting in PrB_6, assuming the EFG to be collinear with H_{int}, and the broadening of 1–2 mm/sec compared with the

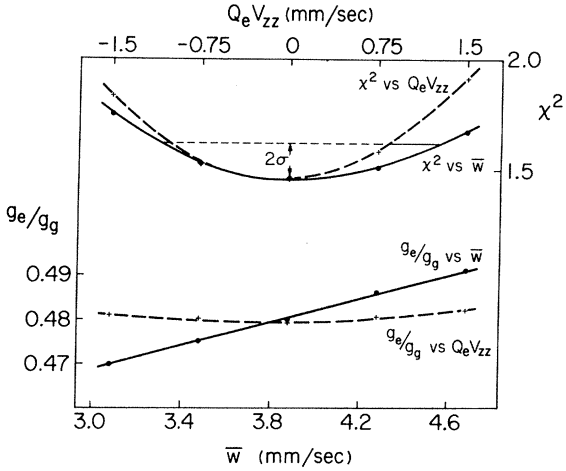

FIG. 5. The upper curves show the values of χ^2 obtained in fitting the PrB_6 data with various values of the excited-state quadrupole splitting (dashed curve) and with various fixed values of the average component width (solid curve). The lower curves give the corresponding best-fit values of the g-factor ratio.

natural line width in Pr_2O_3 and PrF_3, correspond to an upper limit of 0.30 b for the quadrupole moment of the excited state. Kisslinger and Sorensen[14] predict the value 0.28 b.

Isomer Shifts

All the compounds listed in Table I are trivalent except for PrO_2 and Pr_6O_{11}. The outer electronic structure of Pr^{3+} is $4f^2 5s^2 5p^6$ and that of Pr^{4+} is $4f^1 5s^2 5p^6$. The extra $4f$ electron in the former compounds increases the shielding of the $5s$ and $5p_{1/2}$ electrons, thereby decreasing the total electron density at the nucleus. Thus, the more positive isomer shifts of tetravalent relative to trivalent compounds indicates a larger charge radius of the excited state than of the ground state.

Following Brix *et al.*[16] we extrapolate the results of ^{151}Eu isomer-shift analysis to the present case. They reported a difference in electron density at the site of the nucleus in Eu^{2+} and Eu^{3+} ions in gases of 1.9×10^{26} cm^{-3}. More recent optical-shift experiments[17] have shown that the electron densities in solids are larger than in free atoms. In the following discussion the value $|\psi(0)|^2_{\text{solid}}/|\psi(0)|^2_{\text{atom}} = 2.06$, adopted by Kienle, Kalvius, and Ruby[18] in reviewing isomer-shift data, is used. Calculations reported by Freeman[19] indicate that the difference in electron density at the nucleus for Pr^{2+} and Pr^{3+} is about 12% smaller than the difference for Eu^{2+} and Eu^{3+}. This effect is largely cancelled by the decrease in $4f$ orbital radius which occurs when an electron is removed from each of the above Pr ions to obtain Pr^{3+} and Pr^{4+}, so one may assume

$$|\psi_0(Pr^{3+})|^2 - |\psi_0(Pr^{4+})|^2 \simeq |\psi_0(Eu^{2+})|^2 - |\psi_0(Eu^{3+})|^2 .$$

The isomer shift between the most-ionic trivalent

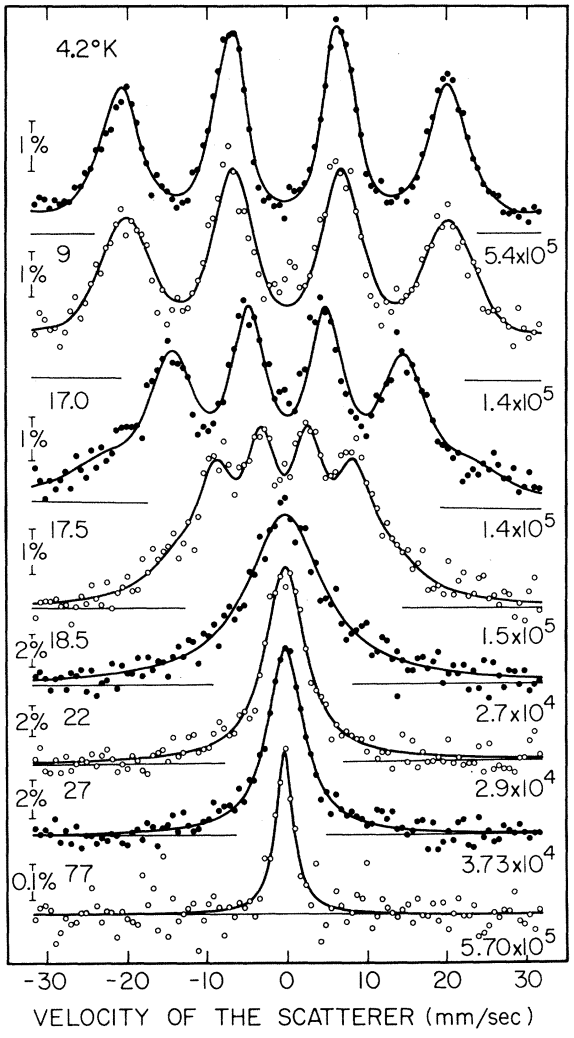

FIG. 6. Temperature dependence of the hyperfine spectrum of PrB_6. At the right of each spectrum the number of counts per channel in the nonresonant background is indicated. The bars to the left give the vertical scales in terms of the background. The temperature of the scatterer is also shown to the left of each curve. The source temperature was 4.2°K for all but the bottom spectrum where it was 77°K.

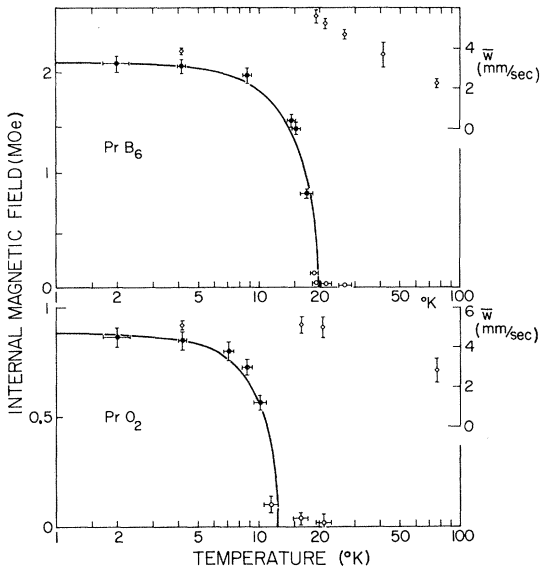

FIG. 7. Temperature dependence of the internal magnetic fields in PrB_6 and PrO_2. The solid circles represent values of the field determined in a fitting procedure where the widths of the Zeeman components were free to be adjusted. The open circles represent field values obtained with the widths of the Zeeman components constrained in the fitting procedure. The curves are least-squares adjusted Brillouin functions ($J=4$ for PrB_6 and $J=\frac{5}{2}$ for PrO_2). The squares plotted for temperatures above the Néel point represent the widths of Lorentzian curves fitted to the broadened velocity spectra. The average component width at 4.2°K is indicated for comparison.

compound PrF_3 and tetravalent PrO_2 is 0.97 ± 0.08 mm/sec. If these compounds are assumed to be purely ionic and the above estimate of the difference in electron densities is made, giving $\delta|\psi|^2 = (3.9 \pm 1.5) \times 10^{26}$ cm^{-3}, the change in mean square nuclear-charge radius obtained is $\langle r_e^2 \rangle - \langle r_g^2 \rangle = (6.3 \pm 2.5) \times 10^{-3}$ fm^2. The error includes a 30% uncertainty in the optical-shift data plus an estimate of the uncertainty in extrapolating from the ^{151}Eu electron density.

Compounds with isomer shifts intermediate between those of PrF_3 and PrO_2 are less ionic than PrF_3. One finds, for instance, that the isomer shift of the sesquioxide relative to that of the fluoride is 0.2 mm/sec. This evidence of covalent bonding in Pr_2O_3 indicates that the isomer shift of PrO_2 may by slightly smaller than that expected for a purely ionic tetravalent compound, and thus the value for the change in nuclear radius obtained above may be somewhat too small. Both the intermetallic compound $PrAl_2$ and the compounds PrB_6, PrN, and PrS, which are semiconductors, are expected to have some 6*s* character in the electronic configurations of the Pr^{3+} ions and, therefore, to have positive isomer shifts relative to PrF_3, as observed.

While the relative shifts between different scattering materials are related as expected, the shift between the CeO_2 source and the PrO_2 scatterer is puzzling. Angular-correlation measurements[20] have shown that the ^{143}Pr ions following the decay of ^{143}Ce in CeO_2 are predominantly tetravalent. This should also be valid for the decay of ^{141}Ce. Although the CeO_2 lattice constant is about 1% larger than the PrO_2 lattice constant, and Ce^{4+} differs somewhat in electronegativity from Pr^{4+}, these effects are not expected to produce an isomer shift comparable with that produced by a change in the valency of the ion.

Interference between Rayleigh and Mössbauer scattering could, in principle, produce a false isomer shift between source and scatterer without affecting the relative shifts among scatterers. The false shift divided by the half-width of the resonant line is approximately equal to the ratio of the intensity of the interference term to the Mössbauer term. In the present case, the amplitude for Rayleigh scattering through 180° is so small that the shift in line position is less than 1% of the line width and can be neglected (cf. Appendix).

Internal Fields

The internal magnetic fields measured in compounds which gave resolved Mössbauer spectra at 4.2°K are considerably smaller than the reported[3] free-ion fields (60% in PrB_6, 50% in $PrAl_2$, and 47% in PrO_2). The Pr^{4+} free-ion field, taken to be that of the isoelectronic Ce^{3+} ion without allowing for the extra nuclear charge, is probably underestimated by 5–10%. Despite the departure of these fields from the free-ion values normally observed in magnetically ordered rare-earth compounds, the temperature dependence of the hyperfine interaction in PrB_6 and PrO_2 below the ordering temperature approximates a Brillouin function, although the Néel temperature of 19.8°K deduced for PrB_6 is much larger than the value 7.5°K obtained in bulk-susceptibility measurements.[6] The Pr^{4+} ion exhibits Kramers degeneracy in a cubic lattice, and the PrO_2 spectrum might therefore arise from the paramagnetic hyperfine interaction if the relaxation times are long enough. The Pr^{3+} ion, however, has an even number of electrons, and the spectrum of PrB_6 almost certainly results from antiferromagnetic ordering.

Below the ordering temperature all the components do not have the same width. In the case of PrB_6 the increase in line width is about 6% of the displacement from zero velocity and can be explained in terms of the impurity of the sample, which could give rise to various values of the internal field corresponding to stoichiometric variations. The PrO_2 sample, on the other hand, was very pure and the variation in line width would correspond to a variation in fields of $\Delta H/H \simeq 0.3$. An attempt to explain this broadening in terms of spin-spin relaxation was not satisfactory. Estimation of the relaxation times, which requires a knowledge of the crystal field parameters, was unreliable. When relaxation times were chosen short enough to account for the broadening of the outer peaks the central part of the computed spectrum was found to differ significantly from that observed. With increasing temperature the spectrum collapses without the additional broadening of the outer components or the appearance of a central peak that would be expected if spin-spin relaxation were the dominant mechanism quenching the effective field.

APPENDIX

Velocity Dispersion

A nucleus bound in a scatterer moving with vertical velocity v relative to a stationary source has an effective velocity $v\cos\theta$ for resonant excitation by a γ ray emitted at an angle θ to the vertical (cf. Fig. 1). Consequently, photons scattered at the same time but from different points on the scatterer have different Doppler shifts although they are recorded in the same velocity channel. The resulting velocity dispersion shifts the cen-

troid and broadens and distorts the shape of each component of the velocity spectrum. Properly accounting for these effects is important if accurate values of the g-factor ratio and the hyperfine fields are to be determined. Let $W(\cos\theta)$ be the probability that a γ ray is emitted at an angle θ to the vertical, strikes the scatterer, and, if scattered, is detected. The observed line shape of each component in the scattered spectrum is then given by

$$I(v)=\frac{\Gamma}{2\pi}\int_A^B \frac{W(\cos\theta)}{(v\cos\theta-v_0)^2+\frac{1}{4}\Gamma^2}\,d(\cos\theta)\Big/\int_A^B W(\cos\theta)\,d(\cos\theta), \tag{1}$$

where A and B are the cosines of the largest and smallest accepted emission angles, $\Gamma=\Gamma_{\text{source}}+\Gamma_{\text{scatt}}$ is the full width of the (assumed Lorentzian) component, and v_0 is its resonant velocity. The full spectrum is a properly normalized sum over all such components.

Since the evaluation of $W(\cos\theta)$ in closed form is very difficult with the present geometry, Monte Carlo techniques were used to calculate the relative probability of different γ-ray trajectories through the system. An expansion of the form

$$W(\cos\theta)=a_0+a_1\cos\theta+a_2\cos^2\theta+a_3\cos^3\theta, \quad (A\leq\cos\theta\leq B), \tag{2}$$

was fitted to the Monte Carlo data for each source-scatterer distance h. The change in $W(\cos\theta)$ for small changes in h was investigated so that the effects of finite scatterer thickness, irreproducibility in positioning the scatterer, and drifts in the equilibrium position of the drive motion could be accounted for. It was found that adjustments in A and B which vary like $(dh/h)^2$ account very well for such geometrical changes. The coefficients a_n in Eq. (2) are very insensitive to small displacements. With the above expansion Eq. (1) gives

$$I(v)=\frac{1}{\pi v}\Bigg\{a_3\frac{(B^2-A^2)}{2\alpha}+\left(\frac{a_2}{\alpha}-\frac{2a_3\beta}{\alpha^2}\right)(B-A)+\left[\frac{a_1}{2\alpha}-\frac{a_2\beta}{\alpha^2}+\frac{a_3(3\beta^2-1)}{2\alpha^2}\right]\ln\left[\frac{(\alpha B+\beta)^2+1}{(\alpha A+\beta)^2+1}\right]$$
$$+\left[-a_0-\frac{a_1\beta}{\alpha}+\frac{a_2(\beta^2-1)}{\alpha^2}+\frac{a_3\beta(3-\beta^2)}{\alpha^3}\right]\arctan\left[\frac{\alpha(B-A)}{1+(\alpha B+\beta)(\alpha A+B)}\right]\Bigg\}, \tag{3}$$

where $\alpha=2v/\Gamma$ and $\beta=2v_0/\Gamma$. The values of $I(v)$ calculated from expression (3) have been compared with those obtained by direct evaluation of Eq. (1) by Monte Carlo techniques. They differ by less than 3% at all points in the spectrum but Eq. (3) can be evaluated nearly 100 times faster.

The scattered peaks given by Eq. (3) are centered at $v_0\langle\cos\theta\rangle\simeq v_0(B+A)/2$, where $\langle\cos\theta\rangle$ is the mean value of $\cos\theta$. The second moment (width of the peaks is greater than Γ by an amount proportional to $(2v_0/\Gamma)\times\delta(\cos\theta)\simeq(2v_0/\Gamma)(B-A)/2$, where $\delta(\cos\theta)$ is the variation in $\cos\theta$. The asymmetry (ratio of third moment to second moment) is also proportional to this quantity. This functional form for the component line shape was used in fitting the velocity spectrum obtained when a ^{57}Co source and Fe_2O_3 scatterer were used in the same geometry employed in the ^{141}Pr experiments. Good fits to the data were obtained with the value of Γ for the components equal to the width (0.38 mm/sec) of the Lorentzian components fitted to the transmission spectrum of the same material. The values of $\cos\theta$ and $\delta(\cos\theta)$ which gave the best fit to the spectrum were in good agreement with those obtained in the Monte Carlo calculations.

For the outer lines of the Fe_2O_3 spectrum $2v_0/\Gamma\simeq 42$. The value of this quantity, which is a measure of the distortion, is considerably smaller for all lines in the PrB_6 and PrO_2 spectra. For example, $2v_0/\Gamma\simeq 8$ for the component labeled a in Fig. 2, and about half as large for the corresponding PrO_2 line in Fig. 3. Since Eq. (3) adequately accounts for the large distortions of the Fe_2O_3 spectrum where a transmission spectrum is available for reference, it should accurately account for the effects of velocity dispersion in the less distorted Pr spectra.

Distribution of Fields

If the hyperfine field does not have a unique value for all nuclei, Eq. (1) for the line shape of each component must be extended as follows:

$$I(v)=\frac{\Gamma}{2\pi}\int_A^B\int_{-\infty}^{\infty}\frac{W(\cos\theta)P(v_0-\bar{v}_0)}{(v\cos\theta-v_0)^2+\frac{1}{4}\Gamma^2}\,dv_0\,d(\cos\theta)\Big/\int_A^B\int_{-\infty}^{\infty}W(\cos\theta)P(v_0-\bar{v}_0)dv_0\,d(\cos\theta), \tag{4}$$

where $P(v_0 - \bar{v}_0)$ is the probability function for the distribution of the resonant velocity v_0 about its mean value $\bar{v}_0$. This distribution can correspond either to a finite number of discrete values or to a continuous variation in the resonant energy. Discrete values of the internal field simply increase the number of components used in fitting the data. For continuous distributions numerical integration must often be used to evaluate Eq. (4). In fitting the data obtained in the present experiments, distributions of the form $P(x) = (1 \pm \rho x)e^{-x^2/2\sigma^2}$ as well as rational polynomial forms were used, since they allow easy parametrization of the moments of the field distribution and permit the use of simple Gaussian integration techniques in evaluation of Eq. (4).

Interference with Rayleigh Scattering

The wavelength of the 145-keV radiation from ^{141}Pr is about 100 times smaller than the distance between praseodymium nuclei in the scattering material and interference will occur between Mössbauer scattering and Rayleigh scattering from only the electrons of the same atom. The Mössbauer intensity has the Lorentzian form $I_0/\{1 + [2(v - v_0)/\Gamma]^2\} = I_0/(1 + \epsilon^2)$, and the intensity of the interference term has the dispersion form $I_1\epsilon/(1 + \epsilon^2)$. If $I_1 \ll I_0$ the superposition of these two intensities gives $(I_0 + I_1\epsilon)/(1 + \epsilon^2) \approx I_0/[1 + (\epsilon - I_1/I_0)^2]$, which is a Lorentzian shifted by I_1/I_0. If the Rayleigh scattering is of $E1$ character and the transition is $M1$, one obtains[21] $I_1/I_0 \simeq (1 + \alpha)\beta \times 2F_0 \cos\theta/\lambda\!\!\!^{-}$ where $\alpha = 0.45$ is the internal-conversion coefficient, $\beta \simeq 1.1$ allows for attenuation of the γ rays in the scatterer, θ is the scattering angle, $2\pi\lambda\!\!\!^{-}$ is the resonant wavelength, and F_0 is the form factor of Frantz.[22] The value of F_0 was obtained from the calculated[23,24] differential Rayleigh-scattering cross section. In the present case, although Rayleigh scattering is not predominantly $E1$, its amplitude is so small that the shift in line position produced is less than 1% of the line width. Inclusion of other multipoles can make the angular factor in I_1/I_0 different from $\cos\theta$ but will not significantly change the magnitude of the shift.

Note added in proof: Groves, Debrunner, and De Pasquali[25] have recently reported on the isomer shifts of the 145-keV transition in various praseodymium compounds using Mössbauer scattering. Their final values for isomer shifts of Pr_2O_3, P_6O_{11}, and PrF_3 relative to PrO_2 agree with our values.

Our data was analyzed in terms of Lorentzian as well as various non-Lorentzian line shapes. Non-Lorentzian lines can arise not only from the reasons discussed in the text, but from an interference between the hyperfine levels of the excited nuclear states. It is well known[26] that this interference occurs with a magnetically aligned scatterer. However, it has recently been pointed out[27] that even in the case of a randomly oriented magnetic hyperfine field in the scatterer one gets non-Lorentzian lines. In the limit that the Zeeman splitting between two levels in the excited state, m and m', is much greater than the width of the excited state ($|E_m - E'_m| \gg \Gamma$) the interference is small and one obtains negligible deviations from Lorentzian lines. We find $|E_m - E'_m|/\Gamma \gtrsim 22$ for the PrB_6 scatterer and $E_m - E'_m/\Gamma \gtrsim 9$ for the PrO_2 scatterer; therefore, the interference effect is sufficiently small that our analysis includes it.

---

†Work performed under the auspices of the U. S. Atomic Energy Commission. Prepared under Contract No. AT(04-3)-63 for the San Francisco Operations Office, U. S. Atomic Energy Commission.

[1]C. M. Lederer, J. M. Hollander, and I. Perlman, *Table of Isotopes* (John Wiley & Sons, Inc., New York, 1967), 6th ed.

[2]P. Debrunner and H. Frauenfelder, *Applications of the Mössbauer Effect in Chemistry and Solid-State Physics* (International Atomic Energy Agency, Vienna, Austria, 1966), p.58.

[3]S. Ofer, I. Nowik, and S. G. Cohen, in *Chemical Applications of Mössbauer Spectroscopy,* edited by V. I. Goldanskii and R. H. Herber (Academic Press Inc., New York, 1968), p. 440.

[4]D. D. Cook, B. I. Persson, and M. F. Bent, Bull. Am. Phys. Soc. 14, 1172 (1969).

[5]T. F. Connoly and E. D. Copenhaver, Oak Ridge National Laboratory Report No. ORNL-RM1C7 (Rev.), 1969 (unpublished).

[6]T. H. Geballe, B. T. Matthias, K. Andres, J. P. Maita, A. Cooper, and E. Corenzwit, Science 160, 1443 (1968).

[7]D. Agresti, E. Kankeleit, and B. Persson, Phys. Rev. 155, 1342 (1967).

[8]E. Kankeleit, Rev. Sci. Instr. 35, 194 (1964); in *Mössbauer Effect Methodology,* edited by I. Gruverman (Plenum Press, Inc., New York, 1965), Vol. 1, p. 47.

[9]A. F. Clifford, in *Rare Earth Research II,* edited by K. Vorres (Gordon and Breach Science Publishers, Inc., New York, 1964), p. 45.

[10]Freshly prepared samples were kindly supplied by Professor LeRoy Eyring and his colleagues at Arizona State University, who also analyzed the materials.

[11]M. F. Bent, B. I. Persson, and D. Agresti, Computer Phys. Communications 1, 67 (1969).

[12]V. S. Shirley, in *Hyperfine Structure and Nuclear Radiations,* edited by E. Matthias and D. A. Shirley (North-Holland Publishing Company, Amsterdam, The Netherlands, 1968), p. 998.

[13]A. Arima and H. Horie, Progr. Theoret. Phys. (Kyoto) 12, 623 (1954).
[14]L. S. Kisslinger and R. A. Sorensen, Rev. Mod. Phys. 35, 853 (1963).
[15]S. Wahlborn and J. Blomqvist, Nucl. Phys. A133, 50 (1969).
[16]P. Brix, S. Hüfner, P. Kienle, and D. Qiutmann, Phys. Letters 13, 140 (1964).
[17]J. Grabmaier, S. Hüfner, E. Orlich, and J. Pelzl, Phys. Letters 24, A680 (1967).
[18]P. Kienle, G. M. Kalvius, and L. S. Ruby, in *Hyperfine Structure and Nuclear Radiations*, edited by E. Matthias and D. A. Shirley (North-Holland Publishing Company, Amsterdam, The Netherlands, 1968), p. 971.
[19]A. J. Freeman, in *Hyperfine Structure and Nuclear Radiations*, edited by E. Matthias and D. A. Shirley (North-Holland Publishing Company, Amsterdam, The Netherlands, 1968), p. 75.
[20]P. N. Tandon and H. G. Devare, in *Hyperfine Structure and Nuclear Radiations*, edited by E. Matthias and D. A. Shirley (North-Holland Publishing Company, Amsterdam, The Netherlands, 1968), p. 164.
[21]M. Atac, P. Debrunner, and H. Frauenfelder, Phys. Letters 21, 699 (1966).
[22]W. Frantz, Z. Physik 98, 314 (1936).
[23]S. Brenner, G. E. Brown, and J. B. Woodward, Proc. Roy. Soc. (London) A227, 59 (1954).
[24]C. M. Davisson, in *Alpha-, Beta-, and Gamma-Ray Spectroscopy*, edited by K. Siegbahn (North-Holland Publishing Company, Amsterdam, The Netherlands, 1965), Vol. 1, p. 58.
[25]J. L. Groves, P. Debrunner, and G. De Pasquali, Phys. Letters 33A, 51 (1970), and errata, to be published.
[26]T. A. Tumolillo, Nucl. Phys. A143, 78 (1970).
[27]K. Gabathuler, Diplomarbeit, Swiss Federal Institute of Technology, Zurich, 1970 (unpublished); K. Gabathuler and H. J. Leisi, in the International Conference on Hyperfine Interactions Detected by Nuclear Radiation, Rehovoth, Israel, September, 1970 (unpublished).